Sendai Virus Internal Fusion Peptide: Structural and Functional Characterization and a Plausible Mode of Viral Entry Inhibition†

Jimut Kanti Ghosh,‡,§ Sergio Gerardo Peisajovich,‡ and Yechiel Shai*

Department of Biological Chemistry, The Weizmann Institute of Science, Rehovot 76100, Israel

Received March 15, 2000; Revised Manuscript Received July 13, 2000

ABSTRACT: Viral glycoproteins catalyze the fusion between viral and cellular membranes. The fusion protein (F_1) of Sendai virus has two fusion peptides. One is located at its N-terminus and the other, highly homologous to the HIV-1 and RSV fusion peptides, in the interior of the F_1 protein. A synthetic peptide corresponding to the internal fusogenic domain, namely, SV-201, was found to inhibit virus−cell fusion without interfering with the binding of the virus to the target cells, thus highlighting the importance of this region in Sendai virus-induced membrane fusion. However, its detailed mechanism of inhibition remains unknown. Here, we synthesized a shorter version of SV-201, namely, SV-208, an elongated one, SV-197, and two mutants of SV-201, and compared them functionally and structurally with SV-201. In contrast to SV-201, SV-208 and the two mutants do not inhibit virus−cell fusion. The differences in the oligomerization state of these peptides in aqueous solution and within the membrane, and in their ability to bind to Sendai virions, enabled us to postulate a possible mechanism of viral entry inhibition: SV-201 binds to its target in Sendai virions before the F_1 internal fusion peptide binds to the membrane, therefore blocking the F_1 conformational change required for fusion. In addition, we further characterized the fusogenic activity of the internal fusion peptide, compared to the N-terminal one, and determined its structure in the membrane-bound state by means of fluorescence, CD, and ATR-FTIR spectroscopy. Remarkably, we found that SV-201 and its elongated form, SV-197, are highly potent in inducing fusion of the highly stable large unilamellar vesicles composed of egg phosphatidylcholine, a property found only in an extended version of the HIV-1 fusion peptide. The inhibitory activity of SV-201 and its fusogenic ability are discussed in terms of the "umbrella" model of Sendai virus-induced membrane fusion.

Sendai virus, a member of the Paramyxoviridae family, enters into its host-cell by fusing its envelope with the cellular plasma membrane (*1*−*3*). Two of the six proteins encoded by the viral RNA, namely, hemagglutinin neuraminidase (HN) and the fusion protein (F_0), are envelope proteins responsible for the binding to specific host-cell receptors (*4*) and the subsequent merging of the viral and cellular membranes (*3*), respectively. Fusion proteins from different viral families (e.g., Paramyxo-, Orthomyxo-, and Retroviridae) share conserved features (*5*). Specifically, (i) they are type I integral membrane proteins synthesized as inactive precursors that are cleaved by host-cell proteases to become active; (ii) the newly generated N-terminus contains the fusion peptide, a hydrophobic stretch of amino acids believed to participate in the actual merging of the viral and cellular membranes; and (iii) a heptad repeat adjacent to the N-terminal fusion peptide folds into a trimeric coiled-coil at a certain step during the fusion process (*5*−*7*). However, the ectodomain of paramyxovirus fusion proteins has certain features that result in a more complex picture. First, it is composed of more than 380 amino acids, compared with those of Influenza virus (an orthomyxovirus) and HIV-1 (a retrovirus), which are composed of about 175 amino acids. Second, in addition to the N- and C-terminal heptad repeats, which are similar to those found in retrovirus fusion proteins, an extra leucine zipper is found in the interior of paramyxovirus fusion protein ectodomain (*8*). Third, orthomyxo- and retrovirus fusion proteins are thought to contain only one N-terminal fusion peptide (*5, 9*), whereas paramyxoviruses contain, in addition to the N-terminal fusion peptide, a second one in the interior of the fusion protein (*10*). The importance of the second fusion peptide in Sendai virus-induced membrane fusion was highlighted by the recent finding that a synthetic peptide corresponding to this fusogenic region, namely, SV-201, inhibits the fusion between the virus and red blood cells (*11*).

Several conformational changes characterize the fate of viral fusion proteins. The posttranslational cleavage results in a conformational change manifested by an increase in the exposed hydrophobicity (*12*). Binding to the host-cell receptor induces a second change in conformation that is believed to include the insertion of the fusion peptide into the target

† This research was supported in part by the Henri and Françoise Glasberg Foundation. J.K.G. is the recipient of a Sir Charles Clore postdoctoral fellowship from the Feinberg Graduate School, The Weizmann Institute of Science.

* To whom correspondence should be addressed at the Department of Biological Chemistry, Weizmann Institute of Science, Rehovot 76100, Israel. Tel: 972-8-342711; Fax: 972-8-344112; Email: Yechiel.Shai@weizmann.ac.il.

‡ These authors contributed equally to this work.

§ Present address: Department of Biology, University of California, San Diego, 9500 Gilman Dr., La Jolla, CA 92093-0366.

10.1021/bi0005963 CCC: $19.00
Published on Web 08/30/2000

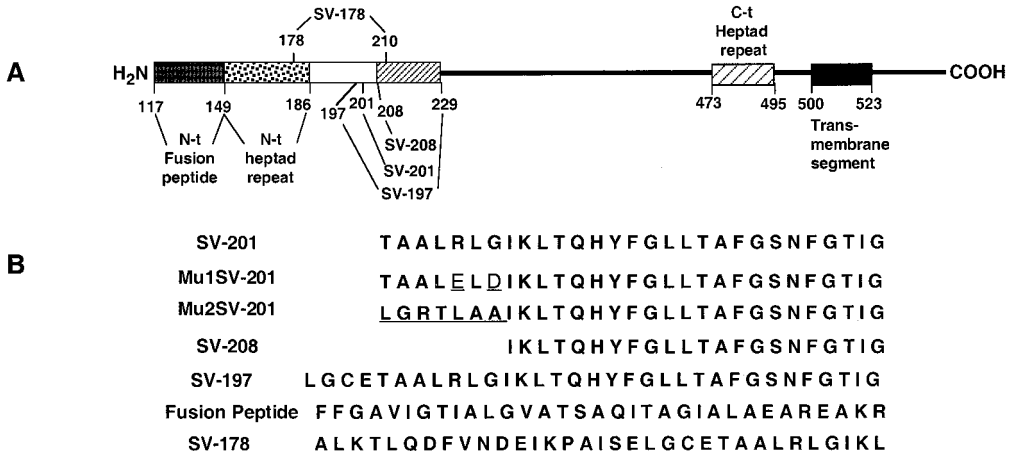

FIGURE 1: (A) Schematic representation of the Sendai virus F_1 protein; (B) amino acid sequences of the peptides used in this study; underlined amino acids are mutated.

membrane and the packing of the C-terminal heptad repeats against the grooves of the coiled-coil formed by the N-terminal heptad repeats, resulting in the structure observed by X-ray crystallography or NMR (*13*−*22*). With paramyxoviruses, a third conformational change is thought to occur, in which the affinity of both the N-terminal and the C-terminal heptad repeats toward the membrane causes the opening of the coiled-coil, accompanied by the binding of these regions to the membrane (*23*).

Some synthetic peptides corresponding to regions of viral fusion proteins show anti-viral activity, suggesting that they can accurately model and interact with functional domains of the viral protein (*24*−*28*). Peptides corresponding to the heptad repeats of HIV-1 (*24*−*26*), Sendai virus (*27, 29*), Respiratory Syncytial virus (*30*), Human Parainfluenza virus type 3 (*30*), Measles virus (*30*), and Newcastle Disease virus (*31, 32*) have been shown to inhibit the fusion induced by the respective virus, presumably by interfering with the conformational change induced by the binding to the host-cell receptors. On the other hand, the inhibitory activity of SV-201, a peptide corresponding to the internal fusion peptide from Sendai virus, has not been fully understood. Since the corresponding region in the fusion protein is thought to play a role in viral entry both before (*11*) and during the actual fusion step (*10*), it is difficult to determine its specific target of inhibition. Interestingly, the HIV-1 fusion peptide was also shown to inhibit cell−cell fusion, presumably by interacting with the fusion domain of gp41 within the membrane (*33*). In an attempt to understand the role of SV-201 in membrane fusion and its mechanism of inhibition, we synthesized a shorter version of SV-201, namely, SV-208, an elongated one, SV-197, and two mutants of SV-201: Mu1-SV-201, in which two conserved amino acids were substituted by two negatively charged amino acids, and Mu2-SV-201, in which the first seven amino acids were scrambled. In addition, we synthesized a peptide that partially overlaps SV-201, namely, SV-178. Figure 1 depicts the sequences of the peptides used in this study. We determined the ability of the peptides to inhibit Sendai virus−red blood cell fusion. In addition, we further characterized the fusogenic activity of the internal fusion peptide, SV-201, toward zwitterionic membranes composed of PC[1] and compared it with those of SV-208, SV-197, Mu1-SV-201, Mu2-SV-201, SV-178, and the Sendai virus N-terminal fusion peptide. We also determined their structure and ability to oligomerize when bound to membranes, by means of fluorescence, CD, and ATR-FTIR spectroscopy. The results presented here help to understand SV-201 mechanism of inhibition and strongly support our recently proposed "umbrella" model of Sendai virus-induced membrane fusion (*10*).

EXPERIMENTAL PROCEDURES

Materials. BOC-amino acids were purchased from Novabiochem AG (Läufelfingen, Switzerland), and BOC-amino acid phenylacetamidomethyl (PAM) resin was obtained from Applied Biosystems (Foster City, CA). NBD-fluoride and other reagents for peptide synthesis were obtained from Sigma. Egg phosphatidylcholine (PC) and phosphatidylserine (PS) were purchased from Lipid Products (South Nutfield, U.K). *N*-(Lissamine-rhodamine B-sulfonyl)dioleoylphosphatidylethanolamine (Rho-PE), *N*-(7-nitrobenz-2-oxa-1,3-diazol-4-yl)dioleoylphosphatidylethanolamine (NBD-PE), *N*-(7-nitrobenz-2-oxa-1,3-diazole) fluoride (NBD-fluoride), and 5-(and 6)-carboxytetramethylrhodamine (Rho) succinimidyl ester were purchased from Molecular Probes (Eugene, OR). All other reagents were of analytical grade. Buffers were prepared using double glass-distilled water. Phosphate-buffered saline (PBS) is composed of NaCl (8 g/L), KCl (0.2 g/L), KH_2PO_4 (0.2 g/L), and Na_2HPO_4 (1.09 g/L), pH 7.3.

Peptide Synthesis and Fluorescent Labeling. The peptides (derived from Sendai virus F1 protein Swissprot entry P04856) were synthesized by a standard solid-phase method on PAM-resin as described (*34, 35*). NBD- and Rho-labeling of the N-terminus of the resin-bound peptides was achieved as previously described (*36*). The peptides were cleaved from the resin by HF treatment and purified by RP-HPLC. Purity (∼99%) was confirmed by analytical HPLC. The peptide compositions were determined by amino acid analysis.

[1] Abbreviations: ATR-FTIR, attenuated total reflection Fourier transform infrared spectroscopy; BOC, butyloxycarbonyl; CD, circular dichroism; DMSO, dimethyl sulfoxide; HF, hydrogen fluoride; LUV, large unilamellar vesicles; NBD-F, 4-fluoro-7-nitrobenz-2-oxa-1,3-diazole; Pam, phenylacetamido-methyl; PC, egg phosphatidylcholine; PBS, phosphate-buffered saline (pH 7.3); RP-HPLC, reverse phase high-performance liquid chromatography; Rho, tetramethylrhodamine; RET, resonance energy transfer; SUV, small unilamellar vesicles; TFA, trifluoroacetic acid; TFE, trifluoroethanol.

Fluorescent labeling did not alter the behavior of the peptides, as indicated previously (*8, 11, 27, 37*).

Virus and Erythrocytes. Sendai virus strain Z was grown in the allantoic sac of 10−11 day old embryonated chicken eggs, harvested 48 h after injection and purified according to Peretz et al. (1974) (*38*). The virus was resuspended in buffer composed of 160 mM NaCl, 20 mM Tricine, pH 7.4, and stored at −70 °C. The activity of virions was expressed in hemagglutinating units (HAU) as described earlier (*38*). Human blood was obtained from a blood bank and used fresh. Prior to use, erythrocytes were washed twice with phosphate-buffered saline (PBS), pH 7.3, and diluted to the desired concentration (% v/v) with the same buffer.

Sendai Virus-Induced Human RBC Hemolysis and Its Inhibition by Peptides. Peptides were added to virion suspensions followed by incubation for 80 min to allow the binding of peptide to virions. Then erythrocytes were added and incubated for 15 min at room temperature to allow the attachment of the virions to the cells. The final incubation was always at 37 °C for 60 min, followed by centrifugation at 5700*g* for 8 min to remove intact cells. In all assays, duplicate samples were used, and two aliquots taken from the supernatant of each sample were placed in two wells of a 96-well plate. The amount of hemoglobin released was monitored by measuring the absorbance of the wells by using an ELIZA plate reader at 540 nm.

Determination of the Ability of Peptides To Bind Sendai Virions. PC SUV (250 μM) were added to 0.1 μM NBD-labeled peptides in the presence or in the absence of Sendai virus (50 HAU). When virions were present, they were preincubated with the peptides for 1 h at room temperature. Inactivation of the virions was achieved by incubation at 65 °C for 20 min. Fluorescence excitation was set at 467 nm and emission at 530 nm; 8 nm slits were used.

Preparation of Lipid Vesicles. Small unilamellar vesicles (SUV) were prepared by sonication of PC as described earlier (*39*). Large unilamellar vesicles (LUV) were also prepared from PC and when necessary with different amounts of Rho-PE and NBD-PE, as follows: dry lipids were suspended in PBS buffer by vortexing to produce large multilamellar vesicles. The lipid suspension was freeze−thawed 6 times and then extruded 20 times through polycarbonate membranes with 0.1 μm diameter pores (Nuclepore Corp., Pleasanton, CA).

Resonance Energy Transfer Measurements. Fluorescence resonance energy transfer was measured using NBD-labeled peptides serving as energy donors and Rho-labeled peptides serving as energy acceptors (*40*). Fluorescence spectra (8 nm slit) were obtained at room temperature, with excitation set at 467 nm (8 nm slit). In a typical experiment, donor peptide (final concentration of 0.06 μM) was added to a dispersion of PC SUV (200 μM) in PBS, followed by the addition of acceptor peptide in several sequential doses. Fluorescence spectra were obtained before and after the addition of the acceptor. The efficiency of energy transfer (E) was determined by measuring the decrease in the quantum yield of the donor as a result of the presence of the acceptor. E was determined experimentally from the ratio of the fluorescence intensities of the donor with (I_{da}) and without (I_d) the acceptor, at the donor's maximal emission wavelength. The percentage of transfer efficiency (E) is given by

$$E = (1 - I_{da}/I_d) \times 100$$

Correction for the contribution of acceptor emission as a result of direct excitation was made by subtracting the signal produced by the acceptor-labeled peptide added to the nonlabeled donor. The contribution of buffer and vesicles was subtracted from all measurements.

Peptide-Induced Lipid Mixing. Lipid mixing of large unilamellar vesicles was measured using a fluorescence probe dilution assay (*41*). Lipid vesicles containing 0.6 mol % each of NBD-PE (energy donor) and Rho-PE (energy acceptor) were prepared in PBS as described before. A 1:4 mixture of labeled and unlabeled vesicles (110 μM total phospholipid concentration) was suspended in 400 μL of PBS, and a small volume of peptide in DMSO was added. The increase in NBD fluorescence at 530 nm was monitored with the excitation set at 467 nm. The fluorescence intensity before the addition of the peptide was referred to as 0% lipid mixing, and the fluorescence intensity upon the addition of Triton X-100 (0.05% v/v) was referred to as 100% lipid mixing.

Membrane Binding Experiments. The degree of peptide association with PC SUV was measured by adding increasing amounts of vesicles to 0.1 μM NBD-labeled peptides dissolved in PBS. The fluorescence intensity was measured as a function of the lipid:peptide molar ratio, with excitation set at 467 nm (8 nm slit) and emission set at 530 nm (8 nm slit). The fluorescence values were corrected by subtracting the corresponding blank (PBS with the same amount of vesicles). The binding isotherms were analyzed as partition equilibria (*42*−*44*), using the formula:

$$X_b^* = K_p^* C_f$$

where X_b^* is defined as the molar ratio of bound peptide per 60% of the total lipid, assuming that the peptides were initially partitioned only over the outer leaflet of the SUV, as has been previously suggested (*43*); K_p^* corresponds to the partition coefficient; and C_f represents the equilibrium concentration of the free peptide in the solution. X_b was calculated by extrapolating F_∞ (the fluorescence signal obtained when all the peptide is bound to lipid) from a double reciprocal plot of F (total peptide fluorescence) versus C_L (total concentration of lipids) (*42*). Knowing the fluorescence intensities of unbound peptide, F_0, as well as bound peptide, F, the fraction of membrane-bound peptide, f_b, could be calculated using the formula:

$$f_b = (F - F_0)/(F_\infty - F_0)$$

Having calculated the value of f_b, it is then possible to calculate C_f as well as the extent of peptide binding, X_b^*. The curves that result from plotting X_b^* versus free peptide, C_f, are referred to as the conventional binding isotherms.

Circular Dichroism (CD) Spectroscopy. CD spectra were obtained using an Aviv 202 spectropolarimeter. The spectra were scanned with a thermostated quartz optical cell with a path length of 1 mm, at 25 °C. Each spectrum was recorded with an averaging time of 10 s, at a wavelength range of 260−195 nm. Fractional helicities (*45*) were calculated as follows:

$$\frac{[\theta]_{222} - [\theta]^0_{222}}{[\theta]^{100}_{222} - [\theta]^0_{222}}$$

where $[\theta]_{222}$ is the experimentally observed mean residue elipticity at 222 nm, and values for $[\theta]^0_{222}$ and $[\theta]^{100}_{222}$, corresponding to 0% and 100% helix content at 222 nm, were estimated at -2000 and $-32\,000$ deg·cm^2/dmol, respectively. Each experiment was repeated twice and found to be in good agreement.

ATR-FTIR Measurements. Spectra were obtained with a Bruker Equinox 55 FTIR spectrometer equipped with a deuterated triglyceride sulfate (DTGS) detector and coupled with an ATR device. For each spectrum, 150 scans were collected, with resolution of 4 cm^{-1}. Samples were prepared as previously described (*46*). Briefly, PC (0.78 mg) alone or with peptide (23 μg) was deposited on a ZnSe horizontal ATR prism (80 × 7 mm). Previous to sample preparations, the trifluoroacetate (CF_3COO^-) counterions which strongly associate with the peptide were replaced with chloride ions through several washings of the peptides in 0.1 M HCl and lyophilizations. This allowed the elimination of the strong C═O stretching absorption band near 1673 cm^{-1} (*47*). Peptides were dissolved in methanol, and lipids in a 1:2 methanol/$CHCl_3$ mixture. Lipid/peptide mixtures or lipids with the corresponding volume of methanol were spread with a Teflon bar on the ZnSe prism. The solvents were eliminated by drying under vacuum for 30 min. Polarized spectra were recorded, and the respective spectra corresponding to pure phospholipids in each polarization were subtracted from the sample spectra to yield the difference spectra. The background for each spectrum was a clean ZnSe prism. Hydration of the sample was achieved by introduction of excess deuterium oxide (^2H_2O) into a chamber placed on top the ZnSe prism in the ATR casting and incubation for 30 min prior to acquisition of spectra. Any contribution of ^2H_2O vapor to the absorbance spectra near the amide I peak region was eliminated by subtraction of the spectra of pure lipids equilibrated with ^2H_2O under the same conditions.

ATR-FTIR Data Analysis. Prior to curve fitting, a straight baseline passing through the ordinates at 1700 and 1600 cm^{-1} was subtracted. To resolve overlapping bands, the spectra were processed using PEAKFIT (Jandel Scientific, San Rafael, CA) software. Second-derivative spectra were calculated to identify the positions of the component bands in the spectra. These wavenumbers were used as initial parameters for curve fitting with Gaussian component peaks. Position, bandwidths, and amplitudes of the peaks were varied until good agreement between the calculated sum of all components and the experimental spectra was achieved ($r^2 > 0.995$), under the following restraints: (i) the resulting bands shifted by no more than 2 cm^{-1} from the initial parameters, and (ii) all the peaks had reasonable half-widths ($<20-25$ cm^{-1}). The relative contents of different secondary structure elements were estimated by dividing the areas of individual peaks, assigned to a particular secondary structure, by the whole area of the resulting amide I band. The experiments were repeated twice and were found to be in good agreement.

Analysis of Polarized ATR-FTIR Spectra. The ATR electric fields of incident light were calculated as follows (*48*):

$$E_x = \frac{2\cos\theta\sqrt{\sin^2\theta - n_{21}^2}}{\sqrt{(1-n_{21}^2)[(1+n_{21}^2)\sin^2\theta - n_{21}^2]}}$$

$$E_y = \frac{2\cos\theta}{\sqrt{1-n_{21}^2}}$$

$$E_z = \frac{2\sin\theta\cos\theta}{\sqrt{(1-n_{21}^2)[(1+n_{21}^2)\sin^2\theta - n_{21}^2]}}$$

where θ is the angle of a light beam to the prism normal at the point of reflection (45°) and $n_{21} = n_2/n_1$ [n_1 and n_2 are the refractive indices of ZnSe (taken as 2.4) and the membrane sample (taken as 1.5), respectively]. Under these conditions, E_x, E_y, and E_z are 1.09, 1.81, and 2.32, respectively. The electric field components together with the dichroic ratio (R^{ATR}, defined as the ratio between absorption of parallel, to a membrane plane, A_p, and perpendicularly polarized incident light, A_s) are used to calculate the orientation order parameter, f, by the formula (*49*):

$$f = \frac{2(E_x^2 - R^{ATR}E_y^2 + E_z^2)}{h(3\cos^2\alpha - 1)(E_x^2 - R^{ATR}E_y^2 - 2E_z^2)}$$

where h is the fraction of transition dipoles in the molecule that belong to the ordered structure of the absorption band whose order parameter has been calculated. Lipid order parameters were obtained from the symmetric (~2853 cm^{-1}) lipid stretching mode, setting $\alpha = 90°$ (*48*). The average angle of orientation of the helical axis with respect to the bilayer normal, γ, is calculated based on the order parameter, with the formula (*49*):

$$f = \frac{1}{2}(3\langle\cos^2\gamma\rangle - 1)$$

RESULTS

Only SV-201 Inhibits Sendai Virus-Mediated Hemolysis. The hemolytic activity of Sendai virus is associated with its fusion with red blood cells (RBC) (*50*). When the virus is incubated with RBC at room temperature, to allow its attachment to the cells, followed by incubation at 37 °C, fusion of the virus with the RBC results in RBC lysis. The extent of lysis can be easily determined by centrifuging the RBC and measuring the absorbance of the supernatant at 540 nm (characteristic of the released hemoglobin). To compare in a reliable way the inhibitory activity of SV-201, its shorter version SV-208, and the mutant peptides, we performed a series of new experiments testing the different peptides under the same conditions, using the same batch of virions and RBC. The inhibitory activity of the different peptides on the Sendai virus-mediated RBC lysis was determined by incubating the virus with each peptide for 80 min, before adding the RBC. As depicted in Figure 2, only SV-201 exhibited a substantial inhibitory activity, whereas the two mutants showed very little inhibition and the short peptide, SV-208, did not show any inhibitory activity. It has been shown before that, at the concentrations used in the inhibitory assay, SV-201 do not inhibit the binding of the virions to the RBC and none of the peptides are hemolytic by themselves (*11*). It was suggested that the inhibitory

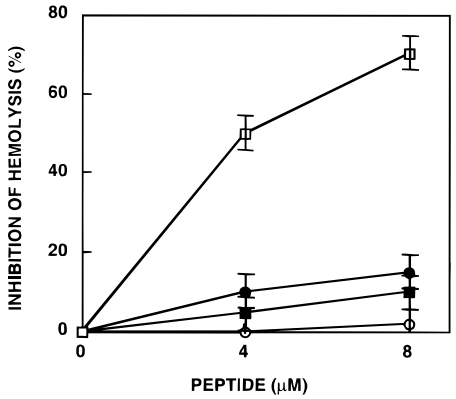

FIGURE 2: Dose response of the inhibition potential of SV-201, SV-208, Mu1-SV-201, and Mu2-SV-201. Various amounts of peptides were added to duplicate samples of virions in 100 μL of PBS and then incubated at room temperature for 80 min. RBC were then added (125 μL of 4%) and incubated for 20 min at room temperature, followed by incubation at 37 °C for 1 h, and finally centrifuged for 8 min at 5700*g*. The inhibition of hemolysis was calculated from the recorded absorbance of the supernatants at 540 nm. Symbols: empty squares, SV-201; filled squares, SV-208; empty circles, Mu1-SV-201; filled circles, Mu2-SV-201.

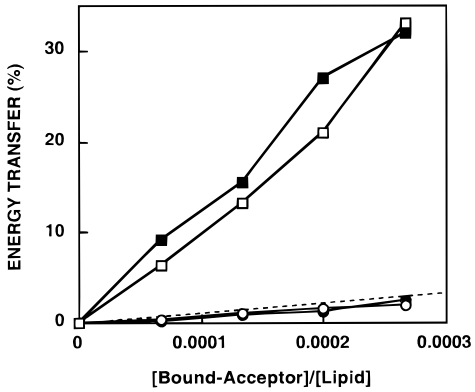

FIGURE 3: Detection of oligomerization of membrane-bound peptides by fluorescence resonance energy transfer. Transfer efficiencies between donor and acceptor SV-201 (empty squares), donor and acceptor SV-208 (filled squares), donor and acceptor Mu1-SV-201 (empty circles), and donor and acceptor Mu2-SV-201 (filled circles) are plotted as a function of [bound acceptor]/[lipid] molar ratio. A theoretical plot showing energy transfer efficiency as a function of the surface density of the acceptors, assuming a random distribution of donors and acceptors, and R_0 = 51 Å, is given for comparison (dashed line). PC SUV were used.

activity of SV-201 (*11*), as well as a peptide corresponding to a leucine-zipper motif located in the ectodomain of the F_1 protein (*8*), is associated with their ability to accurately model and therefore interact with the corresponding domains in the viral protein. Furthermore, SV-201 was reported to oligomerize in aqueous solution (*11*), whereas SV-208 (*10*) and the mutant peptides (*11*) are monomers under these conditions. However, the internal fusogenic region plays a role in the fusion process both in aqueous solution (*11*) and when bound to the membrane (*10*). Therefore, to determine whether SV-201 can interact with its corresponding segment in the F1 protein when it is bound to membranes, we tested the capacity of the peptides to self-associate in their membrane-bound state.

SV-201 and SV-208 Self-Associate in the Membrane. The aggregation states of SV-201, SV-208, and the two mutants were determined by resonance energy transfer measurements. Briefly, peptides labeled at their N-terminus either with NBD, serving as energy donors, or with rhodamine, serving as energy acceptors, were used (*36*). In a typical experiment, a donor peptide (final concentration of 0.06 μM) was added to a dispersion of PC SUV (200 μM) in PBS, followed by the addition of an acceptor peptide in several sequential doses. As depicted in Figure 3, when NBD- and Rho-labeled SV-201 were used as a donor and an acceptor, respectively, dose-dependent quenching of the donor's emission was observed. Similar results were obtained with NBD- and Rho-labeled SV-208. However, when NBD- and Rho-labeled Mu1-SV-201 and Mu2-SV-201 were used, the observed energy transfer was similar to that expected from randomly distributed donors and acceptors (*51*). The lipid-to-peptide ratio was kept high (>3000:1) to create a low surface density of donors and acceptors, thereby reducing the energy transfer between unassociated peptides and ensuring that nearly all the peptides were bound (as discussed later). Note that the acceptor peptide was added only after the donor peptide was already bound to the membrane, thus preventing any association in aqueous solution. These results indicate that both SV-201 and SV-208, but not the mutant peptides, oligomerize in their membrane-bound state. On the other hand, SV-201 is the only peptide able to oligomerize in aqueous solution (*11*) and to inhibit Sendai virus-mediated membrane fusion, thus suggesting that SV-201 blocks the viral entry by interacting with its corresponding domain in the F_1 protein before the internal fusion peptide binds to the membrane. To confirm this hypothesis, we determined whether SV-201 was able to interact with Sendai virions in the absence of target cells in an specific manner.

SV-201 Interacts with Sendai Virions in the Absence of Target Cells. The ability of SV-201 to interact with Sendai virions in an specific manner was determined utilizing NBD-labeled SV-201. The assay was developed with the assumption that binding of NBD-SV-201 to virions will decrease the amount of free NBD-labeled peptide in solution that can bind to phospholipid vesicles. Therefore, the increase in NBD fluorescence upon addition of vesicles is expected to be lower when the labeled peptide was previously incubated with virions than that observed in the absence of virions. As shown in Figure 4, the fluorescence of membrane-bound NBD-SV-201 preincubated with Sendai virus is only 26% of that corresponding to membrane-bound NBD-SV-201 in the absence of virions. This indicates that most of the peptide was bound to the virions and therefore was not able to interact with the phospholipid vesicles. On the other hand, when the peptides were treated with inactivated virions (preincubated at 65 °C for 20 min), the final fluorescence was 3 times higher than that reached when active virions were used. This suggests that SV-201 only binds to active virions. Furthermore, NBD-SV-208 binding to virions was about 2 times lower than that of NBD-SV-201, and no significant differences were observed when activated or inactivated virions were used, suggesting that NBD-SV-208 binds to virions in a nonspecific manner. The ability of SV-201 to specifically bind to Sendai virions in the absence of target cells strongly suggests that the interaction of SV-201 with its target in the virions occurs before the host-cell receptor-induced conformational change in the F_1 protein.

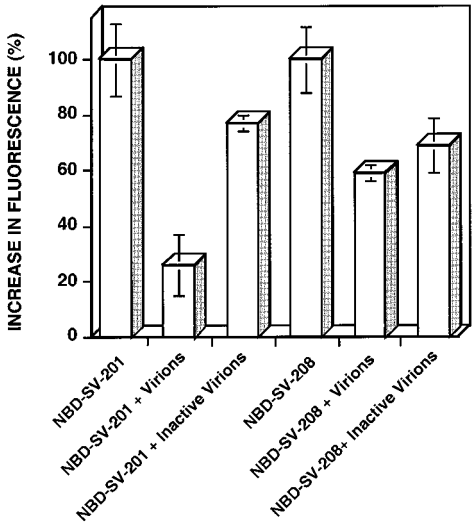

FIGURE 4: Determination of the ability of the peptides to bind Sendai virions. PC SUV (250 μM) were added to 0.1 μM NBD-labeled peptides in the presence or in the absence of Sendai virions (50 HAU). When virions were present, they were preincubated with the peptides for 1 h at room temperature. Inactivation of the virions was achieved by incubation at 65 °C for 20 min. The excitation wavelength was set at 467 nm (8 nm slit) and emission recorded at 530 nm (8 nm slit).

SV-201 Is More Potent Than the N-Terminal Fusion Peptide in Inducing Lipid Mixing of LUV. To further analyze the role of the internal fusion peptide in the process of membrane fusion, we determined the fusogenic activity of the peptides by their ability to induce lipid mixing of LUV (100 nm mean diameter) composed of PC, as revealed by the probe dilution assay (*41*). The dependence of the kinetics and the extent of lipid mixing on the lipid to peptide molar ratio was analyzed. More specifically, in separate experiments, increasing amounts of SV-201, SV-208, SV-197, Mu1-SV-201, Mu2-SV-201, SV-178, and the N-terminal fusion peptide were added to a fixed amount of vesicles. As clearly shown in Figure 5, SV-201 and its elongated form, SV-197, are the only peptides that can induce efficient lipid mixing of neutral membranes composed of PC. In all cases, maximal activities were reached at around 5 min (data not shown). Remarkably, SV-201 and SV-197, the peptides corresponding to the internal fusogenic regions, were substantially more active than the 33-residue N-terminal fusion peptide from the same protein. Interestingly, SV-201 and SV-208 have similar activities against negatively charged membranes composed of PG/PC (1:1) (*10*). Differences in the fusogenic activities of SV-197, SV-201, and the shorter SV-208, against neutral and negative membranes, are similar to those reported for the HIV-1 fusion peptide. Whereas the 33-residue HIV-1 fusion peptide was shown to fuse both neutral and negatively charged membranes, a peptide corresponding to only the first 23 residues was shown to induce lipid mixing of negatively charged vesicles exclusively (*37, 52*). Although further experiments are needed to determine why SV-197 is more potent than the shorter SV-201, we can speculate that elongation helps to stabilize SV-201 secondary structure, thus facilitating fusion. Alternatively, the presence of a free cysteine at position 3 in SV-197 may facilitate its oligomerization and subsequently enhance its fusogenic potency.

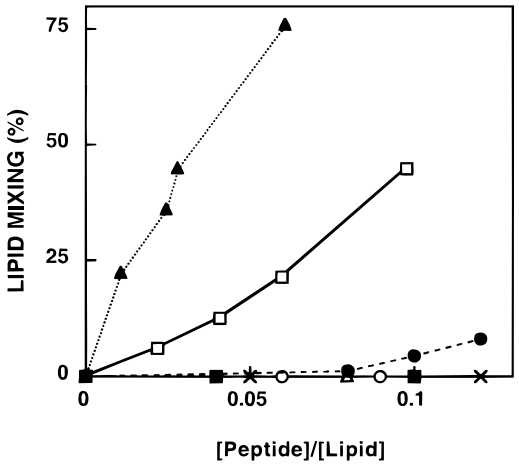

FIGURE 5: Dose dependence of lipid mixing of PC LUV induced by different peptides. Peptide aliquots were added to mixtures of LUV (22 μM), containing 0.6% NBD-PE and Rho-PE, and unlabeled LUV (88 μM) in PBS. The increase in the fluorescence was measured 15 min after the addition of the peptide. The fluorescence intensity upon the addition of reduced Triton-X-100 (0.25% v/v) was referred to as 100%. The excitation wavelength was set at 467 nm (8 nm slit) and emission recorded at 530 nm (8 nm slit). Symbols: SV-201, empty squares; SV-208, filled squares; SV-197, filled triangles; Mu1-SV-201, empty circles; Mu2-SV-201, filled circles; N-terminal fusion peptide, crosses; SV-178, empty triangles.

Binding of the Peptides to PC Vesicles. To determine whether the differences in the fusogenic activity of SV-201, SV-208, and the mutants were due to differences in their membrane-binding abilities, their membrane-binding curves were determined. It has already been shown that the fluorescence emission of NBD increases and shifts to lower wavelengths upon relocation of the NBD moiety to a more hydrophobic environment (*53*). Therefore, the binding curves were determined by measuring the increases in the fluorescence intensities of NBD-labeled peptides, due to membrane binding, as a function of the lipid to peptide molar ratios. The binding curves obtained for SV-201 and the two mutants are similar, reaching saturation at about the same lipid to peptide molar ratios (Figure 6, panel A). On the other hand, the binding curve corresponding to SV-208 suggests a lower affinity of this peptide toward neutral membranes (Figure 6, panel A). Since both SV-208 and the mutant peptides are monomeric in aqueous solution, as revealed by rhodamine dequenching experiments (data not shown), we were able to analyze their binding isotherms as partition equilibria (*44*). The surface partition coefficients were estimated from the initial slopes of the curves shown in Figure 6, panel B (*43*), and were found to be 4.0 ($\pm$0.5) $\times$ 10^4 M^{-1}, 2.1 ($\pm$0.5) $\times$ 10^4 M^{-1}, and 4.9 ($\pm$0.5) $\times$ 10^3 M^{-1}, for Mu2-SV-201, Mu1-SV-201, and SV-208, respectively. Since the values corresponding to the mutant peptides are of the same order, we concluded that the peptides have similar membrane-binding affinities. SV-201 oligomerizes in solution; therefore, its binding isotherm could not be analyzed. However, since its binding curve is similar to those of the mutant peptides, we could estimate that their partition coefficients are similar. In contrast, the partition coefficient of SV-208 is 1 order of magnitude lower, indicating a substantially diminished affinity for PC membranes. From these experiments, we concluded that the differences in fusogenic activity between

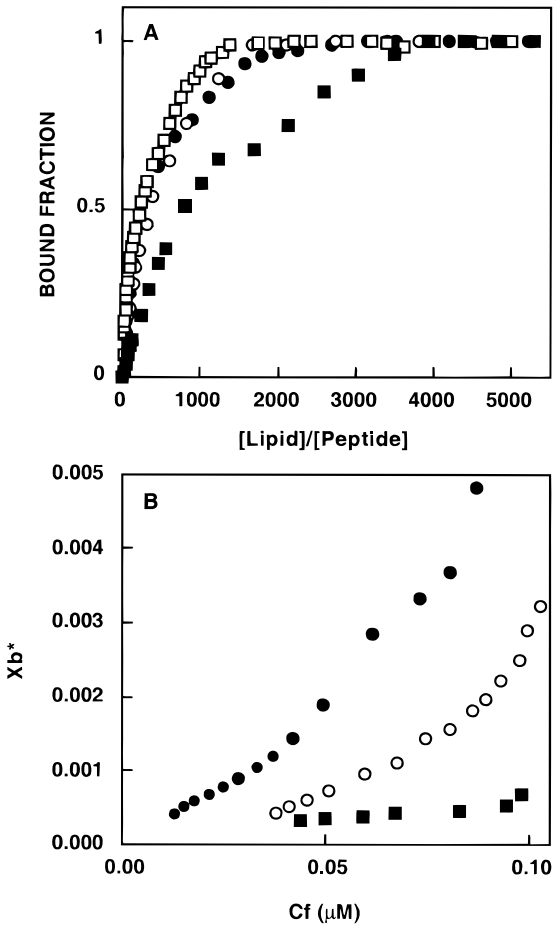

FIGURE 6: Membrane binding activity of the peptides. (A) Increase in the fluorescence of NBD-labeled peptides (0.1 μM) upon titration with PC SUV. Titrations were performed at room temperature in PBS. The excitation wavelength was set at 467 nm (8 nm slit) and emission recorded at 530 nm (8 nm slit). (B) Binding isotherms derived from (A) by plotting X^*_b (the molar ratio of bound peptide/60% of the total lipid) versus C_f (equilibrium concentration of free peptide in solution). Symbols: SV-201, empty squares; SV-208, filled squares; Mu1-SV-201, empty circles; Mu2-SV-201, filled circles.

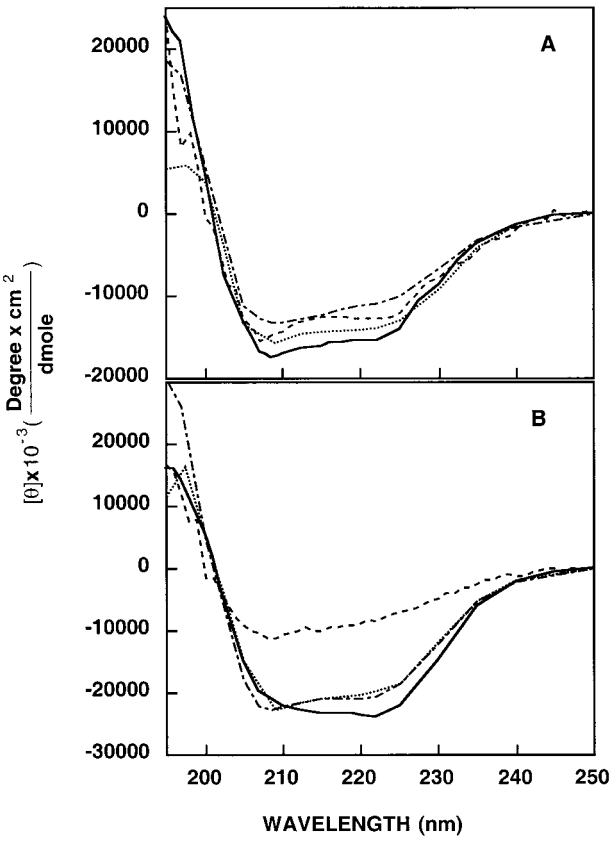

FIGURE 7: CD spectra of the peptides in 1% SDS (A) and 40% TFE (B). Spectra were taken at peptide concentrations of 10 μM. SV-201, solid line; SV-208, dashed line; Mu1-SV-201, dotted−dashed line; Mu2-SV-201, dotted line.

SV-201 and the mutant peptides are not due to a difference in membrane partition, whereas the inability of SV-208 to fuse PC membranes can be partially explained by its lower binding capacity.

Secondary Structures of the Peptides Determined by Circular Dichroism. Structure has been shown to be important for the fusogenic activity of fusion peptides (*54*−*56*). Moreover, membrane binding has been shown to induce stable secondary structure to otherwise unfolded peptides. Therefore, the secondary structure of the peptides in PBS buffer and in membrane mimetic environments such as 1% SDS and 40% TFE was analyzed from their CD spectra. Although we attempted to determine the secondary structure of the peptides when bound to PC vesicles by CD spectroscopy, light scattering caused by the PC vesicles did not allow us to get reliable data. In PBS buffer, the spectra of SV-201, Mu1-SV-201, Mu2-SV-201 (data not shown), and SV-208 (*10*) are typical of random coils, suggesting that the peptides do not adopt stable secondary structures in aqueous solution. On the other hand, as shown in Figure 7, the spectra of the peptides in membrane mimetic environments are indicative of α-helical structures, indicating that binding to the membrane induces stable structures. The spectrum corresponding to SV-208 in 1% SDS, taken from (*10*), is shown for comparison. The fractional helicities in 1% SDS, calculated according to Wu et al. (*45*), are 45% for SV-201, 35% for SV-208 (*10*), 30% for Mu1-SV-201, and 40% for Mu2-SV-201, whereas in 40% TFE they are 73% for SV-201, 23% for SV-208, 63% for Mu1-SV-201, and 60% for Mu2-SV-201. Similarly, Sendai virus N-terminal fusion peptide was found to be 80% α-helical in a similar environment (*55*). Note that SV-208 exhibits a more pronounced α-helical structure in the negatively charged environment of 1% SDS than in 40% TFE, in agreement with its higher binding and fusogenic abilities toward negatively charged membranes, compared with those toward zwitterionic membranes.

Secondary Structures of the Peptides in PC Membranes Determined by FTIR. FTIR spectroscopy has been shown to be a powerful tool to determine the structure and orientation of membrane-bound peptides, and to estimate the effect of the peptides in the lipid order. The spectra corresponding to SV-201 and the two mutant peptides are shown in Figure 8. The relative amounts of different secondary structures, according to Jackson and Mantsch (1995), are listed in Table 1. Since the membrane partition of SV-208 was very low and the FTIR experiment requires a low lipid-to-peptide ratio (100:1), the spectrum of SV-208 was not determined. Deconvolution of the amide I region (1600−1700 cm^{-1}) using PEAKFIT revealed that SV-201, Mu1-SV-201, and Mu2-SV-201 have a main peak at around

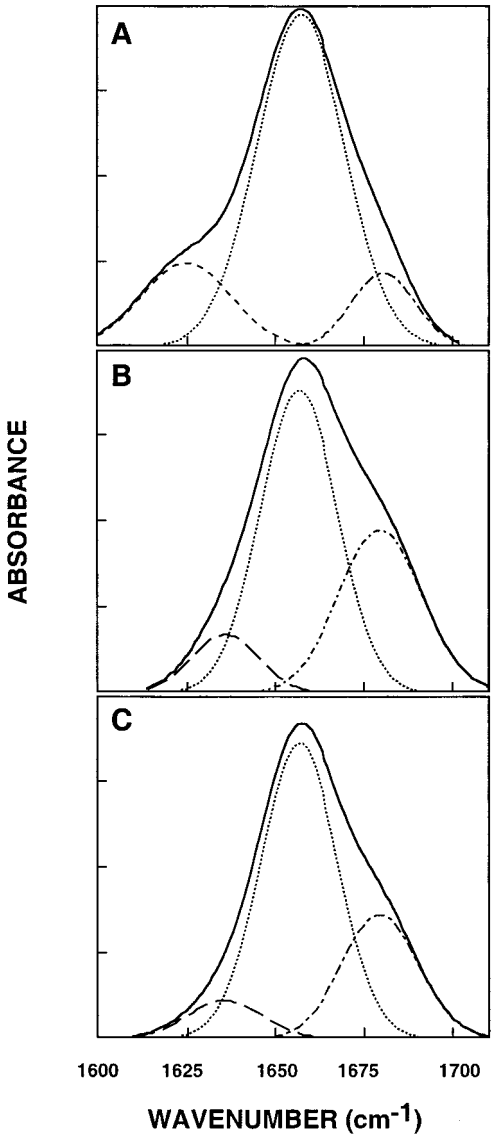

FIGURE 8: FTIR spectra deconvolution of the fully protonated amide I band (1600−1700 cm^{-1}) of SV-201 (A), Mu1-SV-201 (B), and Mu2-SV-201 (C). The component peaks are the result of curve-fitting using a Voigt line shape. The amide I frequencies characteristic of the various secondary-structure elements were taken from Jackson and Mantsch (1995) (*78*). The sums of the fitted components superimpose on the experimental amide I region spectra. The continuous lines represent the experimental FTIR spectra after Savitzky−Golay smoothing; the broken lines represent the fitted components. A 100:1 lipid:peptide molar ratio was used.

1656 cm^{-1} in dry bilayers, suggesting a predominant α-helical structure. This was confirmed by H/D exchange: incubation with D_2O shifted the main peaks to 1651, 1649, and 1648 cm^{-1} in the case of SV-201, Mu1-SV-201, and Mu2-SV-201, respectively. The deconvoluted spectrum of SV-201 has another component at around 1625 cm^{-1} that shifted only to around 1624 cm^{-1} in the presence of D_2O. Although this peak can be assigned either to β-sheet or to aggregated strands, we believe that the small shift may indicate a very compact structure and therefore we assigned the peak to aggregated strands. A third component at around 1680 cm^{-1} can be assigned either to an antiparallel β-sheet, to aggregated strands, or to turns. Deconvolution of the amide I of both mutants revealed very similar spectra. The main component at 1656 cm^{-1}, which shifted to 1648−1649 cm^{-1} after incubation with D_2O, was assigned to an α-helical structure. The second component at 1631−1632 cm^{-1}, which shifted to 1625−1626 cm^{-1} after incubation with D_2O, was assigned to β-sheet. A third component at 1679 cm^{-1} became two components after incubation with D_2O, one at 1667−1668 cm^{-1} and the other at 1681−1682 cm^{-1}. This may suggest that the component at 1679 cm^{-1} before incubation with D_2O is actually an "average" of two peaks that were resolved after incubation with D_2O. However, we cannot rule out the possibility that incubation with D_2O partially altered the secondary structure of the peptides. The component at 1667−1668 cm^{-1} was assigned tentatively to turns, whereas the peak at 1679−1681 cm^{-1} can correspond to antiparallel β-sheet or aggregated strands. It should be noted that the fractional helicities calculated from the CD spectra in 40% TFE are in good agreement with those calculated from the FTIR spectra in PC multibilayers. The SV-201 spectrum has a higher content of aggregated strands compared with the mutant peptides, in accordance with the ability of SV-201 to self-assemble both in solution and in the membrane.

Orientation of the Phospholipid Membrane and Effect of Peptide Binding on Acyl Chain Order. The orientation of the lipid membrane was determined by polarized ATR-FTIR spectroscopy. The symmetric [$\upsilon_{sym}(CH_2)$ ∼2850 cm^{-1}] and the antisymmetric [$\upsilon_{antisym}(CH_2)$ ∼2920 cm^{-1}] vibrations of lipid methylene C−H bonds are perpendicular to the molecular axis of a fully extended hydrocarbon chain. Thus, measuring the dichroism of infrared light absorbance can reveal the order and orientation of the membrane sample relative to the prism surface. The *R* value based on $\upsilon_{sym}(CH_2)$ for the lipids in the absence of peptides was 1.22 ± 0.02, and the corresponding orientation order parameter, *f*, was calculated to be 0.38 ± 0.01. The data indicated that the phospholipid membrane was well-ordered. The observed antisymmetric and symmetric peaks at ∼2922 and ∼2853 cm^{-1}, respectively, indicate that the membranes were predominantly in a liquid-crystalline phase (*48*), similarly to what is found in biological cell membranes. In light of this, we were able to estimate the effect of the peptides on the multibilayer acyl chain order by comparing the CH_2-stretching dichroic ratios of pure phospholipid multibilayers with those obtained with membrane-bound SV-201, Mu1-SV-201, and Mu2-SV-201. The *R* values based on $\upsilon_{sym}(CH_2)$ and the corresponding order parameters, *f* (Table 2), indicated that incorporating SV-201, Mu1-SV-201, and Mu2-SV-201 into the membrane alters the order of the membrane to about the same extent.

Orientation of the Peptides in Lipid Multibilayers Determined by ATR-FTIR Spectroscopy. Since orientation has been thought to be important for fusion activity (*57*), we determined the orientation of the α-helical region of the peptides within the lipid bilayers by polarized ATR-FTIR spectroscopy. Table 3 summarizes the values of the dichroic ratio, *R*, based on the α-helix amide I absorption in the polarized spectra, the corresponding order parameter *f*, and the "average" angle of orientation of the main axis of the molecule with respect to the bilayer normal. The *R* values were similar for SV-201, Mu1-SV-201, and Mu2-SV-201, and the order parameters f were found to be slightly negative, typical of helices oriented oblique to the membrane surface (*58*).

Table 1: Secondary Structures of the Peptides Incorporated to PC Membranes Determined by FTIR[a]

	SV-201		Mu1-SV-201		Mu2-SV-201	
assignment	ν (cm^{-1})	area (%)	ν (cm^{-1})	area (%)	ν (cm^{-1})	area (%)
dry						
aggregated strands	1624.9 ± 0.1	22 ± 9				
β-sheet			1631.1 ± 0.5	26 ± 6	1632 ± 3	10 ± 3
α-helix	1656.4 ± 0.6	66 ± 5	1655.9 ± 0.7	52 ± 6	1656.1 ± 0.6	60 ± 5
turns/aggregated strands/antiparallel β-sheet	1680.2 ± 0.6	12 ± 5	1679.1 ± 0.6	22 ± 11	1679.6 ± 0.1	30 ± 3
hydrated						
aggregated strands	1623.8 ± 0.7	33 ± 6				
β-sheet			1626 ± 2	35 ± 1	1625 ± 1	19 ± 3
α-helix	1651.2 ± 0.1	57 ± 3	1649 ± 1	49 ± 3	1648.3 ± 0.6	56 ± 5
turns			1668.5 ± 0.6	5 ± 2	1667 ± 1	16 ± 3
antiparallel β-sheet/aggregated strands	1678.3 ± 0.5	10 ± 4	1681.9 ± 0.6	11 ± 8	1681 ± 1	9 ± 1

[a] The lipid to peptide molar ratios were 100:1. Values are given as means ± standard deviations.

Table 2: ATR Dichroic Analysis of Lipid Orientation in Multibilayers

	dry		hydrated	
sample[a]	R^b	f	R	f
PC	1.22 ± 0.02	0.38 ± 0.01	1.29 ± 0.02	0.34 ± 0.01
PC + SV-201	1.29 ± 0.03	0.34 ± 0.02	1.34 ± 0.05	0.31 ± 0.03
PC + Mu1-SV-201	1.29 ± 0.01	0.34 ± 0.01	1.36 ± 0.01	0.30 ± 0.01
PC + Mu2-SV-201	1.26 ± 0.02	0.36 ± 0.01	1.31 ± 0.01	0.33 ± 0.01

[a] The lipid:peptide molar ratios were 100:1. [b] R was calculated based on ν_{sym} ~2853 cm^{-1}.

Table 3: ATR Dichroic Analysis of Peptide Orientation in Multibilayers

sample[a]	R	f	g
PC + SV-201, dry	1.51 ± 0.03	−0.25 ± 0.04	64−68°
PC + SV-201, hydrated	1.62 ± 0.07	−0.22 ± 0.06	61−67°
PC + Mu1-SV-201, dry	1.42 ± 0.03	−0.4 ± 0.1	69−90°
PC + Mu1-SV-201, hydrated	1.55 ± 0.05	−0.30 ± 0.06	65−72°
PC + Mu2-SV-201, dry	1.4 ± 0.1	−0.35 ± 0.09	66−78°
PC + Mu2-SV-201, hydrated	1.61 ± 0.01	−0.23 ± 0.02	63−66°

[a] The lipid:peptide molar ratios were 100:1.

DISCUSSION

The SV-201 Mechanism of Virus−Cell Fusion Inhibition. The region corresponding to the internal fusion peptide of Sendai virus F_1 protein has been postulated to participate in the infection process before it binds to the membrane (*11*), and in the actual fusion step after the membrane-induced conformational change (*10*). Therefore, the target of SV-201 inhibition, namely, the specific step in the fusion pathway blocked by SV-201, has not been fully elucidated. In contrast, peptides corresponding to the C-terminal heptad repeats of HIV-1 (*24*, *26*, *59*), Sendai virus (*27*, *29*), Respiratory Syncytial virus (*30*), Human Parainfluenza virus type 3 (*30*), Measles virus (*30*), and Newcastle Disease virus (*31*) have been shown to inhibit the fusion induced by the respective virus, presumably by binding to the N-terminal heptad repeats, before the C-terminal heptad repeats pack into the grooves formed by the coiled coil. In this way, folding into the putative fusion-active conformation is prevented. On the other hand, the N-terminal fusion peptide of HIV-1 gp41 has been shown to inhibit the fusion between gp160/CD4-expressing cells, presumably by specifically binding to its counterpart in the gp41 N-terminus when inserted into the membrane, thus avoiding the correct oligomerization of the fusion peptide required for membrane merging (*33*, *37*). In the present study, we investigated the inhibitory ability of SV-201 by comparing its activity to that of a shorter version of SV-201, namely, SV-208, and two mutant peptides. The differences in the inhibitory activity, their ability to bind to Sendai virions, and the oligomerization state of these peptides in aqueous solution and within the membrane prompted us to distinguish whether SV-201 inhibits the entry of Sendai virus into the host cell before or after the internal fusion peptide binds to the membrane. Interestingly, both SV-201 and SV-208 were able to oligomerize in the membrane (Figure 3), whereas only SV-201 oligomerized in aqueous solution (*10*, *11*). Furthermore, only SV-201 interacts in a specific manner with active virions in the absence of target cells (Figure 4). If inhibition were accomplished by binding to its corresponding region in the membrane, we would expect both peptides to be inhibitors. On the other hand, if inhibition were achieved by binding to the corresponding region in aqueous solution, we would expect only SV-201 to be inhibitor. Since SV-201 but not SV-208 inhibits viral entry to RBC, we postulate that SV-201 binds to its target, possibly its counterpart in the F_1 protein, before the internal fusion peptide binds to the membrane, thus blocking the receptor-induced conformational change, as depicted in Figure 9. Interaction of SV-201 with other targets in Sendai virus, such as the HN protein, cannot be ruled out. It should be noted that although SV-201 oligomerizes under the conditions used in the inhibition experiment, the oligomerization process is reversible (*11*); therefore, part of the peptides are available to interact with their counterparts in the F1 protein. The fact that SV-208 does not inhibit virus−cell fusion, although it oligomerizes in the membrane, may indicate either that binding to the internal fusion peptide in the membrane is not enough to inhibit fusion or that this region is not accessible after membrane binding.

SV-201 Is Highly Fusogenic Independent of Membrane Composition. Synthetic peptides modeled after the fusogenic regions of several viruses including HIV-1 (*33*, *52*, *56*), SIV (*60*, *61*), Influenza (*62*), Sendai (*63*, *64*), Measles (*65*),

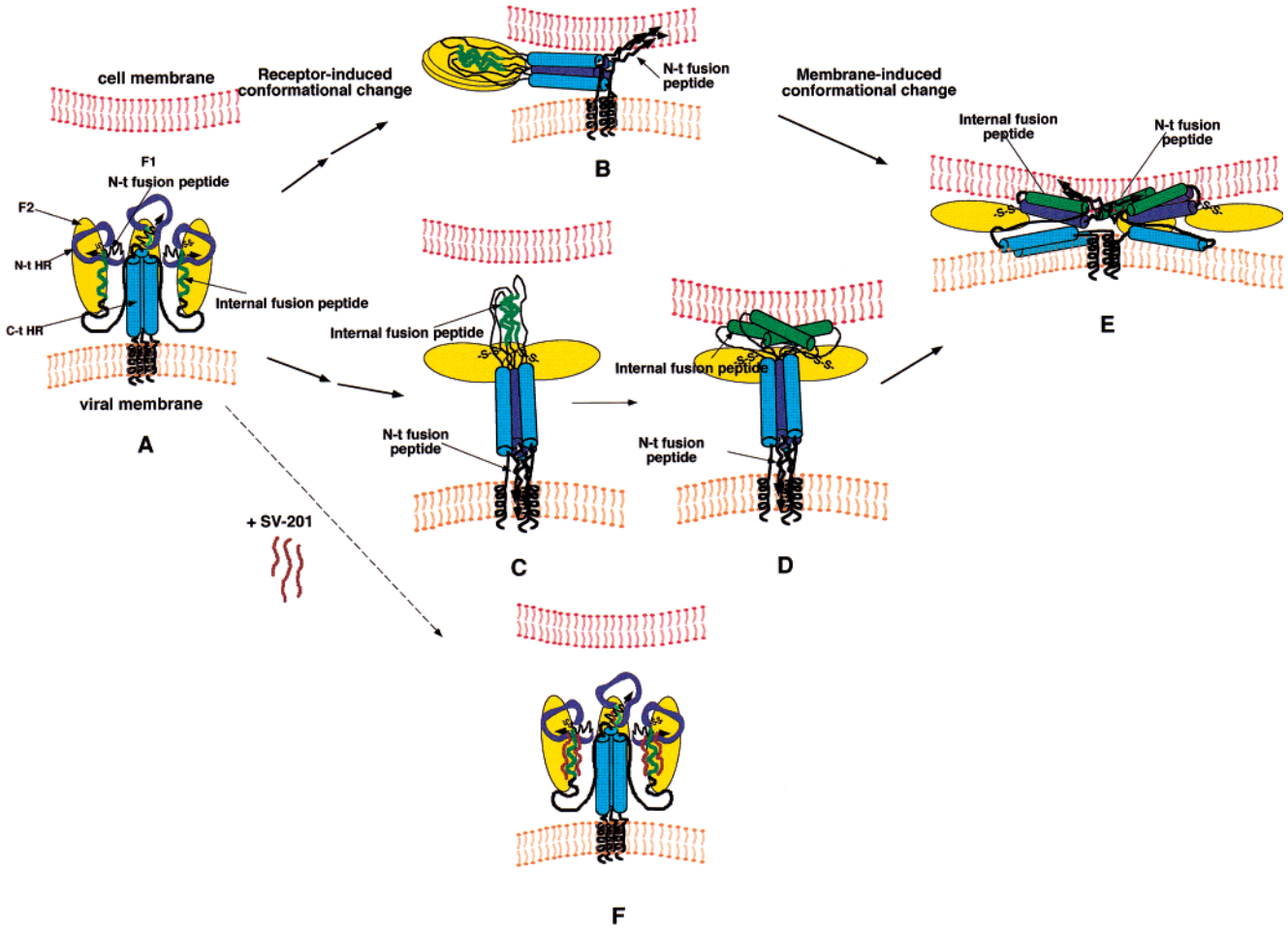

FIGURE 9: Model of SV-201 inhibition of Sendai virus−cell fusion. According to the "umbrella" model of Sendai virus−cell fusion (*10*), binding of the viral surface glycoprotein to cell receptors (A) results in a conformational change of the fusion protein, leading to the formation of a trimeric coiled-coil. Two alternative pathways are possible: the N-terminal fusion peptide inserts into the target membrane first (B); or the initial interaction with the target membrane is achieved by means of the internal fusion peptide, which in this conformation is located on top of the coiled-coil (C and D). After the initial binding, the affinity of both the N-terminal and the C-terminal heptad repeats to the membrane causes the coiled-coil to open (E). SV-201 binds to its counterpart in the F_1 protein before the receptor-induced conformational change (F), preventing the self-assembly of the region corresponding to the internal fusion peptide, and therefore blocks the conformational change required for fusion.

Hepatitis B (*66*), Lassa (*67*), and Ebola (*68*) have been shown to induce fusion of model membranes. Similarly, it has been shown that the region that immediately precedes the transmembrane anchor of HIV-1 fusion protein induces the merging of vesicles (*69*). However, in most of the reported cases, the model membranes were composed, at least in part, of negatively charged lipids or they included at least 30% phosphatidylethanolamine, a factor known to facilitate membrane fusion (*70*). On the other hand, the outer leaflet of eukaryotic membranes is mainly composed of zwitterionic lipids, with a low proportion of phosphatidylethanolamine (*71*). Therefore, the study of peptide-induced fusion of zwitterionic model membranes lacking phosphatidylethanolamine is more relevant to the physiology of viral infection. Here we showed that SV-201, an internal fusion peptide, is able to induce efficient lipid mixing of PC LUV. Interestingly, when negatively charged membranes were used, even the shorter SV-208 was more efficient than the N-terminal fusion peptide in inducing lipid mixing (*10*). The difference in the ability of SV-201 and SV-208 to induce lipid mixing of PC LUV can be partially explained by the lower affinity of SV-208 toward PC membranes. However, the sequence of the extra seven residues located at the N-terminus of SV-201 should be important for fusion, since Mu2-SV-201, which has a similar affinity toward PC membranes and the same amino acid composition as SV-201, is substantially less active than the wild-type peptide. Notably, a similar behavior was reported for the HIV-1 N-terminal fusion peptide (*37*). A segment corresponding to residues 1−33 from HIV-1 gp41 induced fusion of both PS/PC and PC LUV, whereas a peptide corresponding to the first 23 residues was only active against negatively charged vesicles. The high fusogenic activity of SV-197 indicates that elongation of SV-201 to its amino terminus did not disrupt its potency, but rather increased it substantially, suggesting that SV-201 can function as an internal fusion peptide.

A current model for the interaction of fusion peptides with membranes postulates that they are inserted into the membrane at an oblique angle (*57*). This orientation is believed to facilitate membrane destablization [reviewed in (*72*)]. A characteristic of many fusion peptides is that they can readily interconvert between α-helical and *β*-structure conformations (*72*). An α-helical structure was reported for the fusion peptides of Influenza virus, SIV, Newcastle Disease virus,

Measles virus, and the N-terminal fusion peptide of Sendai virus [reviewed in (*73*)]. On the other hand, dissection of HIV-1 fusion peptide showed that its hydrophobic region adopts a predominant β-structure, whereas the consecutive polar segment is mainly α-helical (*74*). Furthermore, an oblique insertion into the membrane has been found for the fusion peptides of Influenza (*75*), SIV (*60*), Bovine Leukemia virus (*76*), Newcastle Disease virus (*77*), Measles virus (*57*), HIV-1 (*33*), and the N-terminal fusion peptide of Sendai virus (*63*). Here, we showed, using both CD spectroscopy in membrane mimetic environments and FTIR spectroscopy in PC multibilayers, that SV-201 and the mutant peptides adopt a predominantly α-helical structure in the membrane. Interestingly, the fractional helicities of the different peptides, calculated from the CD spectra in 40% TFE and from the FTIR spectra in PC multibilayers, are in good agreement. From the analysis of the dichroic ratio, based on the α-helix amide I absorption in the polarized spectra, we determined that SV-201 and the two mutants are in a oblique orientation with respect to the plane of the membrane. Accordingly, the three peptides decrease the lipid order, reflecting a reorganization of the lipid molecules due to the presence of oblique-inserted peptides. Furthermore, in dry bilayers there is a correlation between the α-helical content and the orientation of the peptides and their fusogenic activity. SV-201, which is highly fusogenic, is 66 (±5)% α-helical, and its main axis forms an "average" angle of 64−68° with respect to the bilayer normal; Mu2-SV-201, which has a very low fusogenic ability, is 60 (±5)% α-helical and forms an "average" angle of 66−78°; and Mu1-SV-201, which is not fusogenic, is 52 (±6)% α-helical and forms an "average" angle of 69−90°. This suggests that a decrease in the amount of α-helix or an orientation more parallel to the plane of the bilayer could render the peptides inactive. These observations are in apparent contradiction with the results of Ghosh and Shai (*64*), who demonstrated that a fusogenic peptide named SV-117, comprising the N-terminal fusion peptide and the following N-terminal heptad repeat of the Sendai fusion protein, lied more parallel (71°) than nonfusogenic variants (61° and 66°) to negatively charged PC/PG (1:1) membranes. However, it should be noted that the angle calculated based on the ATR-FTIR spectroscopy data is an "average" of the different angles that may correspond to different α-helical regions along the peptide. In the case of SV-201, the calculated angle corresponds to the average angle of insertion of a 29-residue peptide. On the other hand, SV-117 is a 70-residue peptide that comprises both the N-terminal fusion peptide and the N-terminal heptad repeat. Therefore, the angle determined by ATR-FTIR spectroscopy is only the average of the perhaps different angles that the N-terminal fusion peptide and the heptad repeat are adopting. Indeed, the reported angle of insertion of a peptide corresponding to the N-terminal fusion peptide alone (the first 33 amino acids of SV-117) is 60° (*64*). This suggests that the N-terminal region of SV-117 (the N-terminal fusion peptide) is more inserted into the membrane, whereas the following heptad repeat lies more parallel to the membrane; thus, the average angle determined for SV-117 is 71°. Accordingly, Ben-Efraim et al. reported that a peptide corresponding to the N-terminal heptad repeat alone (the 37 amino acids following the N-terminal fusion peptide) is oriented parallel to the surface of the membrane (*23*).

The ability of SV-201 to induce membrane fusion of PC LUV, in particular in comparison to the inactive N-terminal fusion peptide, strongly supports the "Umbrella" model of Sendai virus−cell fusion [(*10*) and Figure 9]. According to this model, the actual fusion step is not accounted for by the solitary action of an N-terminal fusion peptide, but rather is the consequence of the concerted action of several regions of the F_1 protein. A role for the F_2 protein, which is linked through a disulfide bond to Cys 199, a residue very close to the internal fusion peptide, cannot be ruled out. A detailed understanding of the role played by the N-terminal and the internal fusogenic domains will be needed for fully comprehending the mechanism of paramyxovirus-mediated membrane fusion.

ACKNOWLEDGMENT

We thank Professor Michael Ovadia for the Sendai virions and Kelly Sackett for his help with the virion binding experiments.

REFERENCES

1. Homma, M., and Ohuchi, M. (1973) *J. Virol. 12*, 1457−1465.
2. Scheid, A., and Choppin, P. W. (1977) *Virology 80*, 54−60.
3. Gething, M. J., White, J. M., and Waterfield, M. D. (1978) *Proc. Natl. Acad. Sci. U.S.A. 75*, 2737−2740.
4. Scheid, A., Caliguiri, L. A., Compans, R. W., and Choppin, P. W. (1972) *Virology 50*, 640−652.
5. White, J. M. (1990) *Annu. Rev. Physiol. 52*, 75−97.
6. Stegmann, T., Doms, R. W., and Helenius, A. (1989) *Annu. Rev. Biophys. Biophys. Chem. 18*, 187−211.
7. Skehel, J. J., and Wiley, D. C. (1998) *Cell 95*, 871−874.
8. Ghosh, J. K., Ovadia, M., and Shai, Y. (1997) *Biochemistry 36*, 15451−15462.
9. Gallaher, W. R. (1987) *Cell 50*, 327−328.
10. Peisajovich, S. G., Samuel, O., and Shai, Y. (2000) *J. Mol. Biol. 296*, 1353−1365.
11. Ghosh, J. K., and Shai, Y. (1998) *J. Biol. Chem. 273*, 7252−7259.
12. Hsu, M., Scheid, A., and Choppin, P. W. (1981) *J. Biol. Chem. 256*, 3557−3563.
13. Bullough, P. A., Hughson, F. M., Skehel, J. J., and Wiley, D. C. (1994) *Nature 371*, 37−43.
14. Fass, D., Harrison, S. C., and Kim, P. S. (1996) *Nat. Struct. Biol. 3*, 465−469.
15. Chan, D. C., Fass, D., Berger, J. M., and Kim, P. S. (1997) *Cell 89*, 263−273.
16. Weissenhorn, W., Dessen, A., Harrison, S. C., Skehel, J. J., and Wiley, D. C. (1997) *Nature 387*, 426−430.
17. Malashkevich, V. N., Chan, D. C., Chutkowski, C. T., and Kim, P. S. (1998) *Proc. Natl. Acad. Sci. U.S.A. 95*, 9134−9139.
18. Yang, Z. N., Mueser, T. C., Kaufman, J., Stahl, S. J., Wingfield, P. T., and Hyde, C. C. (1999) *J. Struct. Biol. 126*, 131−144.
19. Weissenhorn, W., Carfi, A., Lee, K. H., Skehel, J. J., and Wiley, D. C. (1998) *Mol. Cell 2*, 605−616.
20. Malashkevich, V. N., Schneider, B. J., McNally, M. L., Milhollen, M. A., Pang, J. X., and Kim, P. S. (1999) *Proc. Natl. Acad. Sci. U.S.A. 96*, 2662−2667.
21. Kobe, B., Center, R. J., Kemp, B. E., and Poumbourios, P. (1999) *Proc. Natl. Acad. Sci. U.S.A. 96*, 4319−4324.
22. Baker, K. A., Dutch, R. E., Lamb, R. A., and Jardetzky, T. S. (1999) *Mol. Cell 3*, 309−319.
23. Ben-Efraim, I., Kliger, Y., Hermesh, C., and Shai, Y. (1999) *J. Mol. Biol. 285*, 609−625.
24. Jiang, S., Lin, K., Strick, N., and Neurath, A. R. (1993) *Nature 365*, 113.
25. Wild, C., Oas, T., McDanal, C., Bolognesi, D., and Matthews, T. (1992) *Proc. Natl. Acad. Sci. U.S.A. 89*, 10537−10541.

26. Wild, C., Greenwell, T., and Matthews, T. (1993) *AIDS Res. Hum. Retroviruses 9*, 1051−1053.
27. Rapaport, D., Ovadia, M., and Shai, Y. (1995) *EMBO J. 14*, 5524−5531.
28. Lawless, M. K., Barney, S., Guthrie, K. I., Bucy, T. B., Petteway, S. R., and Merutka, G. (1996) *Biochemistry 35*, 13697−13708.
29. Ghosh, J. K., Peisajovich, S. G., Ovadia, M., and Shai, Y. (1998) *J. Biol. Chem. 273*, 27182−27190.
30. Lambert, D. M., Barney, S., Lambert, A. L., Guthrie, K., Medinas, R., Davis, D. E., Bucy, T., Erickson, J., Merutka, G., and Petteway, S. R., Jr. (1996) *Proc. Natl. Acad. Sci. U.S.A. 93*, 2186−2191.
31. Young, J. K., Hicks, R. P., Wright, G. E., and Morrison, T. G. (1997) *Virology 238*, 291−304.
32. Young, J. K., Li, D., Abramowitz, M. C., and Morrison, T. G. (1999) *J. Virol. 73*, 5945−5956.
33. Kliger, Y., Aharoni, A., Rapaport, D., Jones, P., Blumenthal, R., and Shai, Y. (1997) *J. Biol. Chem. 272*, 13496−13505.
34. Merrifield, R. B., Vizioli, L. D., and Boman, H. G. (1982) *Biochemistry 21*, 5020−5031.
35. Shai, Y., Bach, D., and Yanovsky, A. (1990) *J. Biol. Chem. 265*, 20202−20209.
36. Rapaport, D., and Shai, Y. (1992) *J. Biol. Chem. 267*, 6502−6509.
37. Pritsker, M., Rucker, J., Hoffman, T. L., Doms, R. W., and Shai, Y. (1999) *Biochemistry 38*, 11359−11371.
38. Peretz, H., Toister, Z., Laster, Y., and Loyter, A. (1974) *J. Cell Biol. 63*, 1−11.
39. Shai, Y., Hadari, Y. R., and Finkels, A. (1991) *J. Biol. Chem. 266*, 22346−22354.
40. Gazit, E., and Shai, Y. (1993) *Biochemistry 32*, 3429−3436.
41. Struck, D. K., Hoekstra, D., and Pagano, R. E. (1981) *Biochemistry 20*, 4093−4099.
42. Schwarz, G., Gerke, H., Rizzo, V., and Stankowski, S. (1987) *Biophys. J. 52*, 685−692.
43. Beschiaschvili, G., and Seelig, J. (1990) *Biochemistry 29*, 52−58.
44. Rapaport, D., and Shai, Y. (1991) *J. Biol. Chem. 266*, 23769−23775.
45. Wu, C. S. C., Ikeda, K., and Yang, J. T. (1981) *Biochemistry 20*, 566−570.
46. Gazit, E., Miller, I. R., Biggin, P. C., Sansom, M. S., and Shai, Y. (1996) *J. Mol. Biol. 258*, 860−870.
47. Surewicz, W. K., Mantsch, H. H., and Chapman, D. (1993) *Biochemistry 32*, 389−394.
48. Ishiguro, R., Matsumoto, M., and Takahashi, S. (1996) *Biochemistry 35*, 4976−4983.
49. Tatulian, S. A., and Tamm, L. K. (2000) *Biochemistry 39*, 496−507.
50. Loyter, A., and Volsky, D. J. (1982) *Cell Surf. Rev. 8*, 215−266.
51. Fung, B. K., and Stryer, L. (1987) *Biochemistry 17*, 5241−5248.
52. Rafalski, M., Lear, J. D., and DeGrado, W. F. (1990) *Biochemistry 29*, 7917−7922.
53. Rajarathnam, K., Hochman, J., Schindler, M., and Ferguson-Miller, S. (1989) *Biochemistry 28*, 3168−3176.
54. Lee, S., Aoki, R., Oishi, O., Aoyagi, H., and Yamasaki, N. (1992) *Biochim. Biophys. Acta 1103*, 157−162.
55. Rapaport, D., Hague, G. R., Pouny, Y., and Shai, Y. (1993) *Biochemistry 32*, 3291−3297.
56. Nieva, J. L., Nir, S., Muga, A., Goni, F. M., and Wilschut, J. (1994) *Biochemistry 33*, 3201−3209.
57. Brasseur, R., Vandenbranden, M., Cornet, B., Burny, A., and Ruysschaert, J. M. (1990) *Biochim. Biophys. Acta 1029*, 267−273.
58. Tamm, L. K., and Tatulian, S. A. (1997) *Q. Rev. Biophys. 30*, 365−429.
59. Kliger, Y., and Shai, Y. (2000) *J. Mol. Biol. 295*, 163−168.
60. Martin, I., Dubois, M. C., Defrise-Quertain, F., Saermark, T., Burny, A., Brasseur, R., and Ruysschaert, J. M. (1994) *J. Virol. 68*, 1139−1148.
61. Colotto, A., Martin, I., Ruysschaert, J. M., Sen, A., Hui, S. W., and Epand, R. M. (1996) *Biochemistry 35*, 980−989.
62. Wharton, S. A., Martin, S. R., Ruigrok, R. W., Skehel, J. J., and Wiley, D. C. (1988) *J. Gen. Virol. 69*, 1847−1857.
63. Rapaport, D., and Shai, Y. (1994) *J. Biol. Chem. 269*, 15124−15131.
64. Ghosh, J. K., and Shai, Y. (1999) *J. Mol. Biol.* 292, 531−546.
65. Yeagle, P. L., Epand, R. M., Richardson, C. D., and Flanagan, T. D. (1991) *Biochim. Biophys. Acta 1065*, 49−53.
66. Rodriguez-Crespo, I., Nunez, E., Gomez-Gutierrez, J., Yelamos, B., Albar, J. P., Peterson, D. L., and Gavilanes, F. (1995) *J. Gen. Virol. 76*, 301−308.
67. Glushakova, S. E., Omelyanenko, V. G., Lukashevitch, I. S., Bogdanov, A. A., Jr., Moshnikova, A. B., Kozytch, A. T., and Torchilin, V. P. (1992) *Biochim. Biophys. Acta 1110*, 202−208.
68. Ruiz-Arguello, M. B., Goni, F. M., Pereira, F. B., and Nieva, J. L. (1998) *J. Virol. 72*, 1775−1781.
69. Nieva, J. L., Gallaher, W. R., Suarez, T., Aguirre, A., and Goni, F. M. (2000) *Biophys. J. 78*, 411A.
70. Chernomordik, L., Kozlov, M. M., and Zimmerberg, J. (1995) *J. Membr. Biol. 146*, 1−14.
71. Jain, M. K. (1988) *Introduction to Biological Membranes*, Second ed., John Wiley & Sons, New York.
72. Epand, R. M. (1998) *Biochim. Biophys. Acta 1376*, 353−368.
73. Pecheur, E. I., Sainte-Marie, J., Bienvene, A., and Hoekstra, D. (1999) *J. Membr. Biol. 167*, 1−17.
74. Peisajovich, S. G., Epand, R. F., Pritsker, M., Shai, Y., and Epand, R. M. (2000) *Biochemistry 39*, 1826−1833.
75. Tatulian, S. A., Hinterdorfer, P., Baber, G., and Tamm, L. K. (1995) *EMBO J. 14*, 5514−5523.
76. Voneche, V., Portetelle, D., Kettmann, R., Willems, L., Limbach, K., Paoletti, E., Ruysschaert, J. M., Burny, A., and Brasseur, R. (1992) *Proc. Natl. Acad. Sci. U.S.A. 89*, 3810−3814.
77. Brasseur, R. (1991) *J. Biol. Chem. 266*, 16120−16127.
78. Jackson, M., and Mantsch, H. H. (1995) *Crit. Rev. Biochem. Mol. Biol. 30*, 95−120.

BI0005963